

Polyimides from an Asymmetric Hydroxyl-Containing Aliphatic-Aromatic Diamine Synthesized via Henry Reaction

Zhiang Wang, Liying Guo, Songyu Han, Haixia Qi, Yusheng Cheng, Feng Liu 

College of Chemistry, Nanchang University, 999 Xuefu Avenue, Honggutan New District, Nanchang 330031, People's Republic of China

Correspondence to: H. Qi (E-mail: hxqi@ncu.edu.cn) or F. Liu (E-mail: liuf@ncu.edu.cn)

Received 23 March 2017; accepted 23 June 2017; published online 00 Month 2017

DOI: 10.1002/pola.28720

ABSTRACT: An aliphatic amino and an aliphatic hydroxyl group have been incorporated via Henry reaction highly efficiently toward the synthesis of a novel asymmetric aliphatic–aromatic diamine 2-amino-1-[4-(5-aminopyridyloxy)phenyl]-1-ethanol (AAP_vP_hE) in three steps. AAP_vP_hE shows good copolymerization reactivity with 4,4'-oxydianiline (ODA) toward different aromatic dianhydrides, especially 4,4'-oxydiphthalic anhydride (ODPA). TGA measurement and mechanical test results show that all polymers maintain the inherent thermal performance and tensile properties, while the glass transition temperatures (T_g 's) by DMA show moderate decrease ranging from 185.5 to 253.3 °C due to the presence of aliphatic segments. The introduction of AAP_vP_hE is found to improve the solubility of the polymers, and the polymer films' optical

transparency with decreased cutoff wavelength (λ_0) ranging from 328 to 370 nm. Comparative studies reveal that the pendant aliphatic hydroxyls in the polymer chains would lead to interchain cross-linking via condensation and secondary weak cross-linking by hydrogen bond depending on different loading of AAP_vP_hE, which result in a fluctuation of hydrophilic–hydrophobic properties, DMA $\tan \delta$ and dielectric constant of the copolymer films. © 2017 Wiley Periodicals, Inc. *J. Polym. Sci., Part A: Polym. Chem.* **2017**, *00*, 000–000

KEYWORDS: asymmetric aliphatic–aromatic diamine; aliphatic hydroxyl; Henry reaction; cross-linking via condensation; hydrogen bond

INTRODUCTION Polyimides (PIs) are a class of high-performance polymers with cyclic imide groups in main chain. Aromatic PIs are well known for their excellent thermal, mechanical performance, and dielectric properties; therefore, widely used in many areas especially in microelectronic.^{1–3} However, aromatic PIs usually suffer from poor solubility and strong intermolecular charge-transfer complexes (CTCs) that results in a strong absorption in UV and visible region and a high dielectric constant (ϵ'), limiting their applications.^{4,5} To overcome these drawbacks, many structural modification methods have been taken such as (1) introducing fluorine, sulfur, and phosphorus substituent and other bulky groups; (2) designing asymmetric structure; and (3) incorporating alicyclic or aliphatic structures.^{2,6–11} All these methods could be capable of improving the PIs' solubility. Recently, the less polarized fluorinated structure and nonaromatic (alicyclic or aliphatic) structures have shown considerable efficiency in reducing CTC and thus dielectric constant (ϵ').^{12–16}

Although there have been concerns about their strong nucleophilicity and basicity during polymerization, the aliphatic

diamines have attracted considerable attention in preparing PIs due to their great industrial significances.^{17,18} Watanabe and Imai explored the approach to synthesize high-molecular-weight polyimides from aliphatic diamines by high-pressure and at high temperature (using ethylene glycol as solvent), respectively.^{19,20} Ueda used tetracarboxylic dianhydrides and trans-1,4-cyclohexyldiamine to prepare high-molecular-weight semiaromatic PAAs in the presence of acetic acid.²¹ Van Mele prepared aliphatic PIs by one step in m-cresol and NMP and studied the odd–even effect of the aliphatic diamine.²² Ward synthesized high-molecular-weight soluble, amorphous, partially aliphatic polyimides by condensing aliphatic diamine with ester acid to sidestep the formation of gel-like nylon salt.²³ *N*-silylation of aliphatic diamine also proved an effective measure to avoid the nylon salt toward the synthesis of high-molecular-weight PIs from aliphatic diamine.²⁴ It should be noteworthy that none of the approaches could apply to all kinds of aliphatic PIs.

Owing to the presence of the localized lone pair of electrons on the sp^2 orbit of nitrogen atom, the heterocyclic pyridine ring offers an advantage over aromatic benzene ring in

Additional Supporting Information may be found in the online version of this article.

© 2017 Wiley Periodicals, Inc.

providing desired properties such as better solubility and mechanical properties.^{13,25,26} Meanwhile, as a closed conjugated ring with 6 π electrons that meets Huckel's rule, the rigid aromatic pyridine helps to maintain the thermal stability when introduced into the polyimide backbone. Herein, we designed a novel asymmetric aliphatic-aromatic diamine 2-amino-1-[4-(5-aminopyridyloxy)phenyl]-1-ethanol (AAP_yP_hE) which bears an aliphatic hydroxyl, an aliphatic amino and an amino attached to a heteroaromatic pyridine ring. Henry reaction was used for the incorporation of the aliphatic amino and aliphatic hydroxyl highly efficiently. To the best of our knowledge, there has scarcely been report on employing Henry reaction to introduce aliphatic segments to modify aromatic diamine for PIs. We envisaged that the asymmetric aliphatic-aromatic structure would lower the dielectric constant, and simultaneously, improve the optical transparency and solubility of the resultant PIs. However, how to balance the reactivity difference between aromatic amino and aliphatic amino or how to find an appropriate dianhydride for effective polymerization needs to be tackled down. Moreover, it would be very interesting to explore how the aliphatic hydroxyls introduced by Henry reaction influence the properties of the polymers as they are pendent to the polymer chains. It naturally occurred to us that the pendent hydroxyls would lead to the cross-linked structure in PIs, thus better strengthening the thermal stability of aliphatic PIs that otherwise would be remarkably sacrificed.^{27,28} In this work, AAP_yP_hE was used to condense with different aromatic dianhydrides and we comprehensively studied the influence of the incorporated AAP_yP_hE to the solubility, optical thermal, dynamic mechanical thermal, surface, and the dynamic dielectric properties of the resulted PIs.

EXPERIMENTAL

Materials

m-Cresol, methanol, ethanol, dichloromethane, *N,N*-dimethylformamide (DMF), *N,N*-dimethylacetamide (DMAc), nitromethane, *p*-hydroxybenzaldehyde, potassium carbonate, triethylamine (TEA), potassium borohydride (KBH₄), nickel(II) chloride hexahydrate (NiCl₂·6H₂O) were purchased from Sinopharm Chemical Reagent Inc., China, and 2-chloro-5-nitropyridine was purchased from Nanjing Chemlin Chemical Inc., China. Commercially obtained 4,4'-oxydianiline (ODA) was recrystallized from ethanol and dried under vacuum at 80 °C overnight before use, 4,4'-oxydiphthalic anhydride (ODPA), 4,4'-(hexafluoroisopropylidene) diphthalic dianhydride (6FDA), 3,3',4,4'-biphenyltetracarboxylic dianhydride (BPDA), 3,3',4,4'-benzophenonetetracarboxylic dianhydride (BTDA) were commercially obtained and dried under vacuum at 150 °C overnight prior to use.

Measurements

IR spectra were recorded on a Perkin Elmer Fourier Transform Infrared spectrometer. Nuclear magnetic resonance (NMR) spectra were measured on a Bruker DRX 400 spectrometer at 400 MHz for ¹H and 100 MHz for ¹³C in DMSO-*d*₆. The melting points were measured with a microscopic

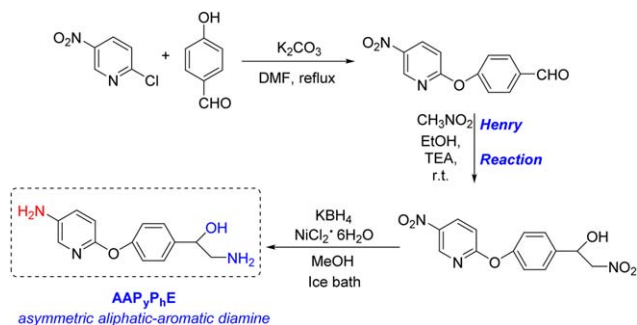
melting point apparatus SGW-X4 (Shanghai Science Apparatus, China) using capillary samples. Inherent viscosities (η_{inh}) were measured with an Ubbelohde viscometer with a 0.5 g dL⁻¹ of DMAc solution at 25 °C. Weight-average molecular weights (M_w) and number-average molecular weights (M_n) were obtained via gel permeation chromatography (GPC) on the basis of polystyrene calibration on a PL-GPC 220 instrument with DMF as an eluent at a flow rate of 1.0 mL min⁻¹. The film samples were immersed in DMF at room temperature for 48 h and the soluble fraction (SF) data of the film samples were measured by dividing the residue weight by the original weight. Wide-angle X-ray diffraction (WAXD) measurement were performed at room temperature on a Bede XRD Di system, using graphite-monochromatized Cu-K α radiation ($\lambda = 0.15405$ nm). Ultraviolet-visible (UV-vis) spectra of the polymer films were recorded on a Shimadzu UV-visible spectrophotometer UV-2450. Contact angle measurements were carried out by using Drop Master 300 Contact AM system (Kyowa Interface Science, Saitama, Japan). Thermogravimetric analysis (TGA) and differential scanning calorimetry (DSC) were conducted with a Perkin-Elmer TGA-2 in flowing nitrogen or in air at a heating rate of 10 °C/min. Dynamic mechanical analyses were conducted with DMA Q800 V20.22 Build 41 using tensile mode at the frequency of 1 Hz. An Instron universal tester model 1122 (GB/T1040.1-2006) was used to study the stress-strain behavior of the film samples at room temperature with a stretching rate of 2.5 mm/min, and the data were the average value of five experiments except for the maximum and the minimum value. Dielectric spectroscopy measurements of the polymer films with the frequency variation in the range of 1-10⁷ Hz at room temperature have been performed using a Novocontrol Dielectric Spectrometer (GmbH Germany), CONCEPT 40. Polymer films electrode with diameter of 10 mm and thickness of 30-70 μ m having gold plated were placed in a flat parallel-plate capacitor, and the amplitude of AC applied voltage was 1 V.

Monomer Synthesis

A nucleophilic substitution reaction between 2-chloro-5-nitropyridine and *p*-hydroxybenzaldehyde was carried out to offer 4-(5-nitropyridyloxy)benzaldehyde, which reacted with nitromethane *via* Henry reaction to obtain aliphatic hydroxyl-functionalized asymmetric aliphatic-aromatic dinitro compound. The subsequent reduction of the dinitro groups was effective enforced by KBH₄ with the catalyst of NiCl₂·6H₂O to generate the corresponding asymmetric aliphatic hydroxyl-containing aliphatic-aromatic diamine monomer AAP_yP_hE. The synthetic route is shown in Scheme 1.

Synthesis of 4-(5-Nitropyridyloxy)Benzaldehyde

Under the atmosphere of nitrogen, to a 100 mL three-necked round-bottomed flask charged with the 2-chloro-5-nitropyridine (3.33 g, 21 mmol) and *p*-hydroxybenzaldehyde (2.4 g, 20 mmol) dissolved in 40mL of DMF, was added potassium carbonate (2.77 g, 20 mmol) at room temperature while stirring for 30 min. The reaction was heated at 45 °C overnight, poured into mixed solvents of ethanol and water



SCHEME 1 The synthesis of 2-amino-1-[4-(5-aminopyridyloxy)-phenyl]-1-ethanol (AAPyPhE). [Color figure can be viewed at wileyonlinelibrary.com]

(volume ratio of 1:2) to get a brown solid, which was recrystallized from petroleum ether and dichloromethane (volume ratio of 1:4), dried to offer pale yellow solid (4.43 g, yield 77.3%). m.p.: 114–116 °C. ¹H NMR (DMSO-*d*₆, ppm): 9.99 (s, 1H), 9.02 (d, *J* = 2.5 Hz, 1H), 8.65 (dd, *J* = 9.0, 2.7 Hz, 1H), 8.00 (d, *J* = 8.4 Hz, 2H), 7.44 (d, *J* = 8.4 Hz, 2H), 7.35 (d, *J* = 9.1 Hz, 1H) (Supporting Information, Fig. S1).

Synthesis Of β-[4-(5-Nitropyridyloxy)Phenyl]Nitroethanol

The β-nitro alcohol was usually prepared by Henry reaction.²⁹ 4-(5-nitropyridyloxy)benzaldehyde (5.2 g, 21.2 mmol) was added into a 50 mL flask with 20 mL ethanol, then nitromethane (1.7 mL, 31.8 mmol) and TEA (0.3 mL, 0.1 mol) was added. The reaction was stirred at room temperature for 12 h, then filtered, recrystallized with ethanol, dried to give white crystals (4.38 g, yield 67.4%). m.p.: 131–133 °C. ¹H NMR (DMSO-*d*₆, ppm): 9.00 (t, *J* = 5.0 Hz, 1H), 8.69–8.50 (m, 1H), 7.68–7.41 (m, 2H), 7.36–7.06 (m, 3H), 6.15 (d, *J* = 4.8 Hz, 1H), 5.43–5.21 (m, 1H), 4.88 (dd, *J* = 12.4, 2.7 Hz, 1H), 4.60 (dd, *J* = 12.3, 10.1 Hz, 1H) (Supporting Information, Fig. S1).

Synthesis of 2-Amino-1-[4-(5-Aminopyridyloxy)Phenyl]-1-Ethanol (AAP_yPhE)

The reduction of asymmetric aromatic–aliphatic dinitro compound into the diamine in this work adopted the method as reported by John O. Osby.³⁰ To a 100 mL three-necked round-bottomed flask containing NiCl₂·6H₂O (1.56 g, 6.56 mmol) and sonicated KBH₄ (1.08 g, 19.68 mmol) in ice bath, was added β-[4-(5-nitropyridyloxy)phenyl]nitroethanol (2 g, 6.56 mmol) and KBH₄ (2.46 g, 45.92 mmol) slowly. The reaction was maintained in an ice bath overnight, then concentrated, purified by column chromatography eluted by mixed CH₃OH and CH₂Cl₂ with volume ratio of 1:50 to offer yellowish-brown solid (1.31 g, yield 81.6%). m.p.: 116–119 °C. Elemental analysis (%): calcd.: C, 63.61; H, 6.16; N, 17.13; found: C, 63.17; H, 5.88; N, 17.26.

The ¹H signals and ¹³C signals in NMR spectrum are shown in Figures 1 and 2. ¹H NMR (DMSO-*d*₆, ppm): 7.51 (d, *J* = 2.0 Hz, 1H), 7.24 (d, *J* = 7.9 Hz, 2H), 7.03 (dt, *J* = 23.4, 11.7 Hz, 1H), 6.87 (d, *J* = 7.7 Hz, 2H), 6.68 (dd, *J* = 24.2, 8.2 Hz, 1H),

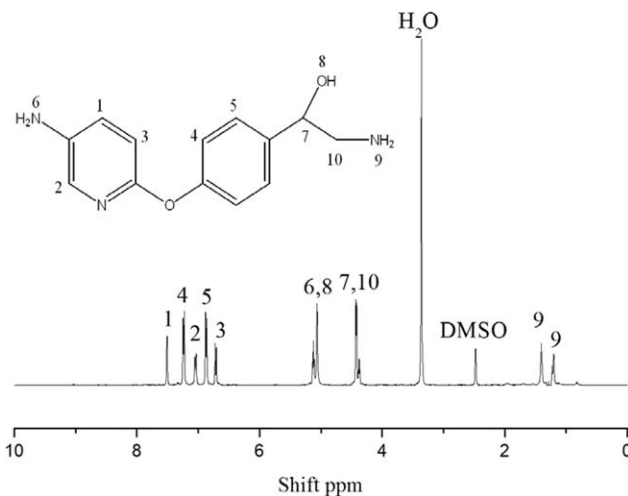


FIGURE 1 The ¹H NMR spectrum of AAP_yPhE.

5.20–4.98 (m, 3H), 4.49–4.30 (m, 3H), 1.38 (d, *J* = 19.4 Hz, 1H), 1.21 (d, *J* = 10.0 Hz, 1H).

¹³C NMR (DMSO-*d*₆, ppm): 155.37 (s), 154.16 (s), 142.24 (s), 137.51 (s), 132.75 (s), 128.20 (s), 125.74 (s), 119.15 (s), 113.05 (s), 62.94 (s), 40.13 (s).

Polymer Synthesis

For powder preparation, the polymerizations of AAP_yPhE with different dianhydrides including BPDA, BTDA, OPA, and 6FDA were carried out by one-step approach, as illustrated by condensation of AAP_yPhE with 6FDA below. Under the atmosphere of nitrogen, to a three-necked flask charged with a Dean-Stark separator, was added AAP_yPhE (1 g, 4.0767 mmol) in 30 mL *m*-cresol and then 6FDA (1.811 g, 4.0767 mmol) at room temperature under magnetic stirring for 30 min. The reaction were then refluxed for 3 h, cooled to room temperature, then precipitated by pouring into ethanol, washed by hot ethanol three times, and dried to offer yellow powders.

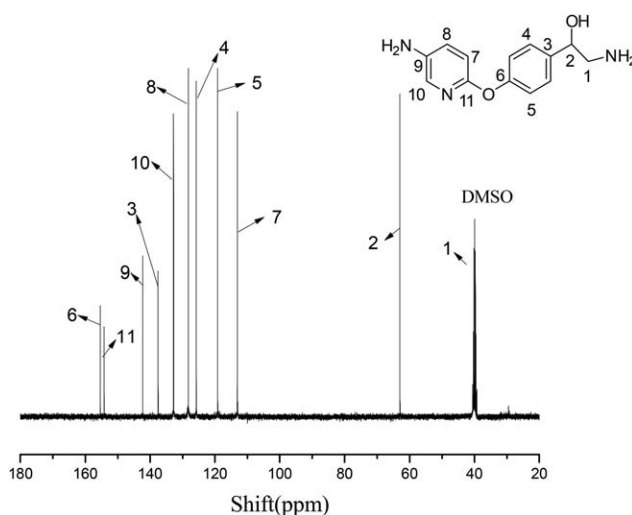
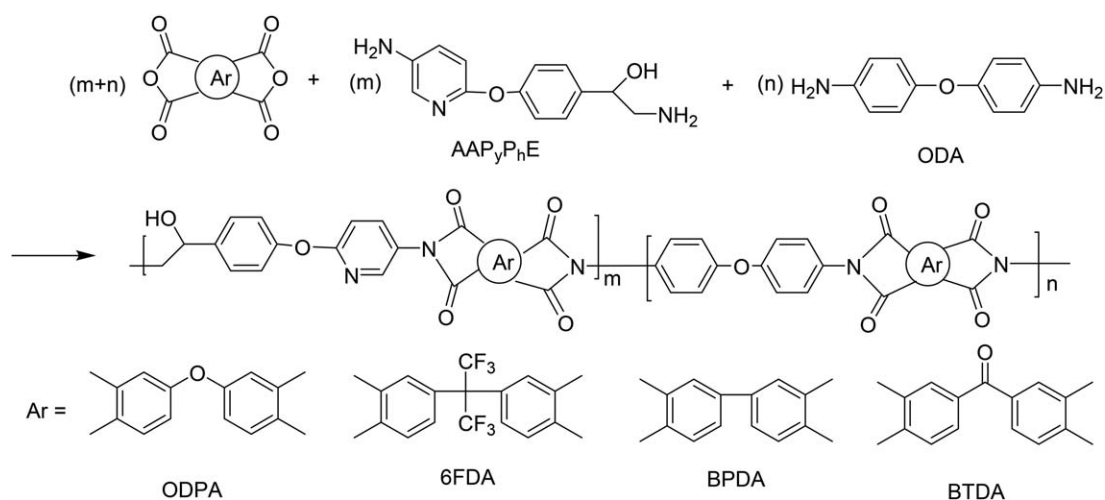


FIGURE 2 The ¹³C NMR spectrum of AAP_yPhE.



SCHEME 2 The synthesis of the polyimides from AAP_yP_hE (for homopolymer powder preparation: $n = 0$; for copolymer film preparation: $m/(m + n) = 0, 0.05, 0.10, 0.20, 0.30, 0.50, 0.75$, respectively).

For film preparation, polymerizations of the combined diamines of AAP_yP_hE and ODA in different ratio with equimolar BPDA, or BTDA, or ODPDA and or 6FDA were conducted by two-step polycondensation. As an illustration, ODPDA (0.3794 g, 1.223 mmol) dissolved in 2.6 g DMAc in a 25 mL flask under nitrogen, and then equal molar of diamine mixtures composed of AAP_yP_hE and ODA were added cautiously to avoid salt solid. The reaction was stirred for 12 h at room temperature, then poured the viscous liquid onto a clean glass plate, thermally treated at 80 °C/5 h, 100 °C/1 h, 150 °C/1 h, 200 °C/1 h, 250 °C/1 h to enforce imidization, and stripped from glass plate by soaking in hot water to offer PI film. Seven copolyimide films were prepared from ODPDA, coded as OPI- x ($x = 0, 5, 10, 20, 30, 50, 75$) according to different molar content of AAP_yP_hE in the diamine mixtures which is 0%, 5%, 10%, 20%, 30%, 50%, and 75%, respectively. Excepted for OPI-7 which presented as brittle film, all OPI- x were flexible films with good tensile strength. For comparison, two copolymer films for each case of BPDA, BTDA, and 6FDA were prepared, coded as PPI- x ($x = 0, 20$), TPI- x ($x = 0, 20$), and FPI- x ($x = 0, 20$) according to the molar content of AAP_yP_hE in the diamine mixtures which is 0% and 20%, respectively.

The synthesis of the polyimides was shown in Scheme 2. As seen in Supporting Information, Figures S2 and S3, all the polymers had the typical absorption bands in IR (cm^{-1}) spectra as at 2924 (saturated C—H stretching), 1785 (C=O asymmetric stretching of imide), 1727 (C=O asymmetric stretching of imide), 1393 (C—N stretching), 1254 (C—O—C stretching), and 719 (imide ring deformation).

RESULTS AND DISCUSSION

The Solubility and Thermal Properties of the Homopolymer Powders

The solubility, thermal properties, and GPC data of the homopolymer powders are summarized in Table 1. All the powders are confirmed as amorphous structure (see WAXD diagrams in Supporting Information, Fig. S4), and most of them are soluble in typical polar solvents such as NMP, DMAc, DMF, THF, cresol, and chlorinated solvent (Chloroform). The general good solubility of the PIs might originate from asymmetrical aromatic-aliphatic backbone structure, which disrupted the polymer chain packing and inhibited the interchain CTC.³¹ 6FDA-AAP_yP_hE and BPDA-AAP_yP_hE show good solubility in all tested solvents at room temperature,

TABLE 1 The Solubility, Thermal Properties, and GPC Data of PI Powders

PIs	Solubility ^a							Thermal properties				GPC		
	NMP	DMAc	DMF	DMSO	<i>m</i> -Cresol	THF	CHCl ₃	T_{d5} (°C)	T_{d10} (°C)	Char Yield (%)	T_g^b (°C)	M_n (KDa)	M_w (KDa)	PDI
ODPA-AAP _y P _h E	+	+	+	+	+	+h	+h	371	414	51.0	221	11.6	15.4	1.33
6FDA-AAP _y P _h E	+	+	+	+	+	+	+	346	394	49.6	126	6.82	8.69	1.27
BPDA-AAP _y P _h E	+	+	+	+	+	+	+	335	387	51.2	145	5.83	8.67	1.49
BTDA-AAP _y P _h E	+	+	+	+	+	±	±	340	393	53.3	125	4.59	6.69	1.46

^a +, soluble; +h, soluble on heating; ±, partially soluble on heating; −, insoluble on heating.

^b Determined by DSC.

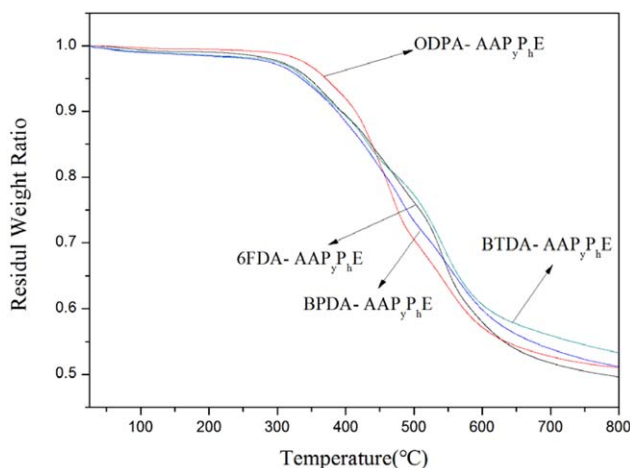


FIGURE 3 The TGA curves of the PI powders. [Color figure can be viewed at wileyonlinelibrary.com]

which could be due to the fluorinated bulky bistrifluoromethylene linkage between two phenyls in 6FDA and the seemingly rigid yet twisted biphenyl structure in BPDA. However, it is unexpected that the flexible sp^3 -oxygen-linked ODPA rather than the planar rigid BTDA shows the poor solubility when condensed with $AAP_{yPh}E$. That may be attributed to the smaller molecular weight of BTDA- $AAP_{yPh}E$ than ODPA- $AAP_{yPh}E$. Owing to the high basicity of aliphatic amino in $AAP_{yPh}E$, nylon salt was formed during polymerization for both dianhydrides, while ODPA offers greater flexibility in that polymerization would proceed much further to give higher molecular weight polymer, other dianhydrides including 6FDA, BPDA, and BTDA lead to rigid backbone that would trap the nylon salt and prevent high polymerization degrees. As indicated by GPC data in Table 1, ODPA- $AAP_{yPh}E$ presents larger molecular weight than 6FDA- $AAP_{yPh}E$, BPDA- $AAP_{yPh}E$, and BTDA- $AAP_{yPh}E$ do.

The thermal properties of PI powders evaluated by TGA and DSC both at heating rate of 10 °C/min under N_2 are shown

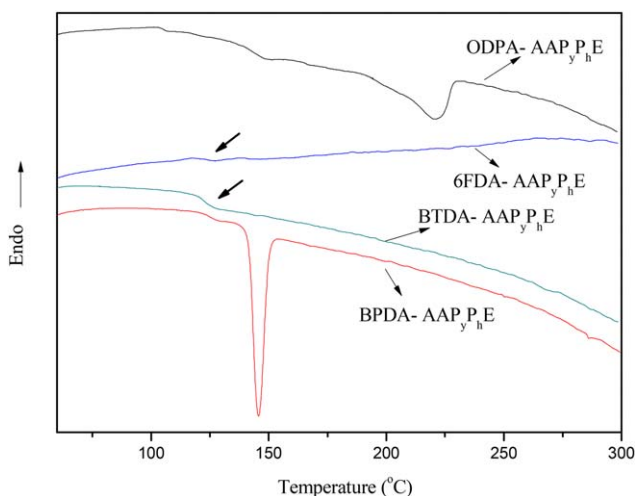


FIGURE 4 The DSC curves of the PI powders. [Color figure can be viewed at wileyonlinelibrary.com]

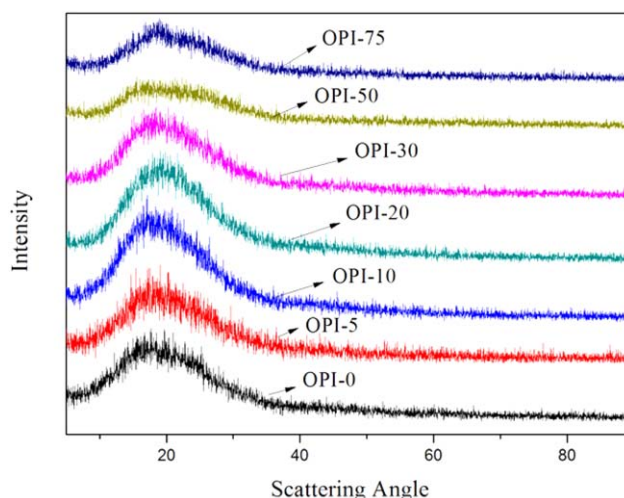


FIGURE 5 The X-ray diffraction diagrams of OPI-x films. [Color figure can be viewed at wileyonlinelibrary.com]

in Figures 3 and 4. The results are summarized in Table 1, with T_{d5} ranging from 335 °C to 371 °C, T_{d10} from 387 °C to 414.5 °C, char yield from 49.6% to 53.3%. It is found that $AAP_{yPh}E$ -ODPA has the best thermal properties and its T_g by far exceeds those of the other three PIs, which, similarly to the case of solubility, could be explained by the higher molecular weight polymer formed by $AAP_{yPh}E$ condensed with ODPA than the other dianhydrides. The above comparisons between polyimides from different aromatic dianhydrides reveal the sufficient condensation reactivity of $AAP_{yPh}E$ toward ODPA when even adopting traditional imidization approach. Therefore, ODPA was adopted as the desired dianhydride toward $AAP_{yPh}E$ in the following parts in this work.

The Solubility, WAXD, and Optical Properties of the Copolymer Films

Figures 5 and 6 show the wide-angle X-ray diffraction (WAXD) spectra of all PI films of OPI-x, TPI-x, BPA-x, and

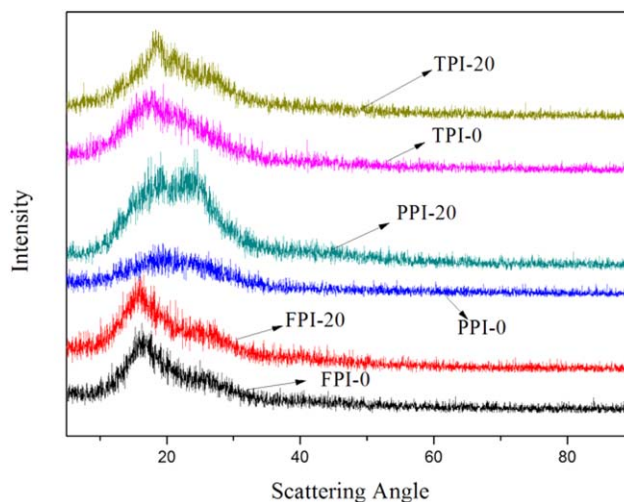


FIGURE 6 The X-ray diffraction diagrams of FPI-x, PPI-x, and TPI-x films. [Color figure can be viewed at wileyonlinelibrary.com]

TABLE 2 The Viscosity, Solubility, WAXD, and Optical Properties of the PI Films

PIs	η_{inh}^a (dL/g)	Solubility ^b							WAXD		Optical properties	
		DMSO	THF	CHCl ₃	m-Cresol	DMAc	NMP	DMF	2θ (°)	d -Spacing (Å)	T_{500} (%) ^c	λ_0 (nm) ^d
OPI-0	1.17	–	–	–	+	+	+	+h	18.9	4.7	72.1	378
OPI-5	1.06	–	–	–	+	+	+	+h	18.4	4.8	83.3	365
OPI-10	0.95	–	–	–	+	+	+	+h	18	4.9	75.6	380
OPI-20	0.92	+h	–	–	+	+	+	+h	17.8	5.0	76.2	369
OPI-30	0.97	+h	–	–	+	+	+	+	17.5	5.1	80.1	374
OPI-50	0.89	+h	+h	–	+	+	+	+	17.3	5.1	75.9	381
FPI-0	1.14	±	+–	–	+	+	+	±	16.5	5.4	80.3	382
FPI-20	0.86	+h	+h	–	+	+	+	+h	15.8	5.6	74.9	370
PPI-0	1.23	±	–	–	+	+h	+	–	20.5	4.3	73.7	404
PPI-20	0.85	+h	+h	–	+	+	+	+h	19	4.7	61.7	445
TPI-0	1.15	–	–	–	+	–	+	–	17.7	5.0	63.5	439
TPI-20	0.79	+	+h	–	+	+h	+	+h	17.8	4.9	55.6	435

^a The inherent viscosity of PAA.

^b +, soluble at room temperature; +h, soluble after heating; ±, partially soluble on heating; –, insoluble.

^c Transmittance at 500 nm.

^d UV–vis cutoff wavelength.

FPI-x series, and all the films present an amorphous state. The average interchain spacing distance (d -spacing) values were calculated from scattering angles (2θ) based on Bragg's equation $n\lambda = 2d\sin\theta$ ($n = 1$, $\lambda = 1.54$ Å), as summarized in Table 2. It is shown that except for the films of TPI-x series, the scattering angles of the films generally decrease with the increasing molar content of AAP_yP_hE for all series, and the d -spacing values present gradual increase which contributes to the enhanced solubility due to the more ready solvation at enlarged polymer interchain distance. The enhancement in solubility could be accounted for by the increased flexibility of polymer backbone due to the presence of the aliphatic ethylene structure in AAP_yP_hE that inhibits chain packing and interchain charge transfer as well.

As seen in Table 2 and Figure 7, λ_0 values of OPI-x range from 365 to 381 nm and OPI-5 exhibits the best optical transparency with 83.3% of T_{500} and 365 nm of λ_0 , which exceed those of OPI-0 (72.1% and 378 nm), indicating that the addition of AAP_yP_hE helps to improve the optical properties of the polymers. The enhancement in optical properties could be attributed to the effects of the aliphatic segments and the asymmetric alternating pyridine and phenyl structure of AAP_yP_hE moieties on breaking the conjugation and weakening the CTC. The variation of AAP_yP_hE loading amount shows fluctuated effects on the optical properties properly due to the film thickness difference and the different presence of the aliphatic hydroxyls pendent to the polymer chains which will be investigated in details in the following parts of this paper. The introduction of 20% molar content of AAP_yP_hE show different effects on the optical properties of FPI-x, PPI-x, and TPI-x (Supporting Information, Fig. S5), and that may be because of the different structural characteristic (such as fluorinated or rigid structure) of the dianhydrides and different polymerization degree as well.

The Surface Properties and Water Absorption of the Copolymer Films

Water contact angle (θ) measurements were carried out for OPI-x and FPI-x films, as shown in Supporting Information, Figure S6. According to eq 1, $+\cos\theta = 2(\gamma_s/\gamma_1)^{1/2} \exp[-\beta(\gamma_1/\gamma_s)2]$, where both γ_1 and β are constant at room temperature, γ_s could be calculated from the determined θ value,^{32,33} and the results together with the water absorptions are summarized in Table 3. It is shown that the values of water contact angle (θ) and surface tension (γ_s) of the films display a fluctuation with the variation of molar content of AAP_yP_hE. For OPI-x series, with the molar content of AAP_yP_hE increasing from 0 (OPI-0) to 10 (OPI-10), the θ decreases from 77.9° to 52.9°, and γ_s undergoes a corresponding increase from 36.7 to 54.1 mN/m, indicating that

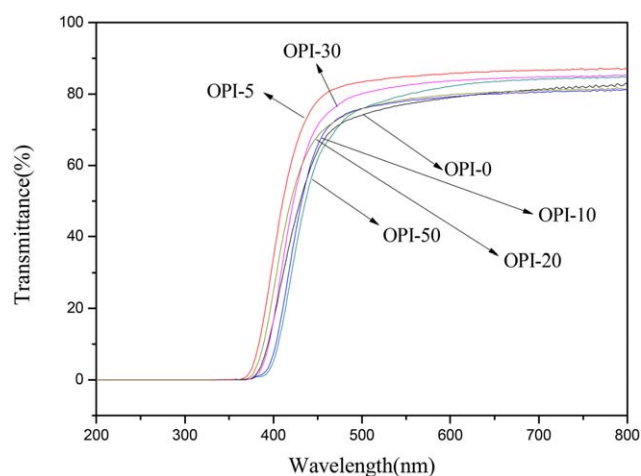


FIGURE 7 The UV–vis spectra of the OPI-x films. [Color figure can be viewed at wileyonlinelibrary.com]

TABLE 3 The Surface Water Contact Properties and Water Absorption of the PI Films

Entries	PIs							
	OPI-0	OPI-5	OPI-10	OPI-20	OPI-30	OPI-50	FPI-0	FPI-20
θ (°) ^a	77.9	67.4	52.9	73.9	57.1	60.7	87.4	65.3
γ_s (mN/m) ^b	36.7	42.4	54.1	38.7	50.1	47.1	32.7	43.6
W_0	0.0363	0.0370	0.0346	0.0343	0.0355	0.0340	0.0371	0.0353
W	0.0367	0.0375	0.0352	0.0347	0.0361	0.0345	0.0374	0.0358
WA ^c	1.14	1.23	1.65	1.16	1.56	1.47	0.92	1.33

^a Equilibrium contact angle was measured at ambient temperature and double distilled water as solvent for a time period of 120 s depending on the stability of the drop, and the data were the average value of 10 experiments.

^b Surface energy, obtained by Owen equation and contact angle.

^c WA(water absorption) (%) = $(W - W_0)/W_0 \times 100\%$; where W is the weight of the polymer sample after immersed in water for 96 h at room temperature and W_0 is the weight of the polymer sample after being dried in vacuum at 100 °C for 8 h.

the introduction of hydroxyl groups by adding AAP_yP_hE effectively increases the hydrophilicity of the PI films. However, with the molar content of AAP_yP_hE continuously increasing to 20% (OPI-20), the film surface properties reverse sharply to a remarkable increase in hydrophobicity with a maximum θ value (73.9°) and a minimum γ_s value (38.7 mN/m). This reversal at OPI-4 is presumed to result from the synergistic effects of the increased presence of aliphatic ethylene structure and the interchain cross-linking *via* condensation of the hydroxyls, which largely eliminated the wetting effect of the hydroxyls and turning the film surface to hydrophobic. However, as the molar content of AAP_yP_hE continues to increase, the presence of free hydroxyl groups would increase because the cross-linked structure acted as a rigid matrix and hindered the condensation for pendent hydroxyl groups at a remote distance. So OPI-30 was more hydrophilic than OPI-20 as indicated by smaller θ value (57.1° vs 73.9°) and larger γ_s value (50.1 vs 38.7 mN/m). When the molar content of AAP_yP_hE further increases, the increasing number of exposed hydroxyl groups would be capable of forming interchain hydrogen bond that turns the polymer OPI-50 into secondary weak cross-linking structure and leads OPI-50 to be more hydrophobic than OPI-30, as evidenced by the comparison of θ and γ_s value.

Owing to the presence of two trifluoromethyl groups, 6FDA could be used to increase the hydrophobicity nature of the traditionally less hydrophobic polyimide composed of repeated polar and hydrophilic imide rings. As examined in this work, FPI-0 derived from 6FDA and ODA shows superior hydrophobicity to ODA equivalent OPI-0. Similar to OPI-*x* series, the incorporation of the aliphatic hydroxyl-containing 20% molar content of AAP_yP_hE leads to an increase of hydrophilicity of 6FDA-based PI films' surface.

Mechanical and Thermal Properties and Cross-Linking Degree of the Copolymer Films

The mechanical properties of all PI films were measured, and the tensile stress-strain curves are provided in Supporting Information, Figure S7. As summarized in Table 4, except for the fragile OPI-75, ODA-based OPI-*x* series show tensile

strengths at break of 89.35–170.73 MPa, elongation at break of 8.33–10.82%, and tensile modulus of 1.35–2.28 GPa. As compared with OPI-0, the addition of AAP_yP_hE with any molar content generally leads to an improvement in mechanical properties of OPI-*x* in terms of tensile strength, modulus, and elongation at break, inferring that asymmetric aromatic-aliphatic segments in AAP_yP_hE helps to strengthen the mechanical properties of the films. The improvement in mechanical properties by adding AAP_yP_hE to flexible dianhydride ODA-ODA PI film is believed to be associated with the interchain cross-linking and the presence of pyridine ring as well, which combinably increase the polymer backbone rigidity and toughen the films. Similar to the effects of the surface properties as discussed above, the variation of molar content of AAP_yP_hE shows the fluctuated effects on the mechanical properties of OPI-*x* series, with the maximum value of mechanical data appearing at OPI-10. Similarly, the introduction of AAP_yP_hE with molar content of 20% was found to increase the tensile properties of 6FDA-based FPI-20 film. Whereas, the incorporation of AAP_yP_hE with 20% molar content to rigid dianhydride BPDA- and BTDA-based PI films leads to a decrease in tensile properties. Because ODA and 6FDA are dianhydrides of flexible structure, yet BPDA and BTDA are rigid, we tend to believe that the cross-linking structure caused by hydroxyls condensation in AAP_yP_hE was moderate and so helpful to increase the mechanical properties for OPI and FPI series, but may aggravate the rigidity of polymer backbones for PPI and TPI series into fragile structures, thus reducing their tensile properties.

The DMA $\tan \delta$ curves for OPI-*x* series is shown in Figure 8, and the DMA $\tan \delta$ curves for the other series are shown in Supporting Information, Figure S8 and the TGA curves for all the films shown in Supporting Information, Figure S9. As summarized in Table 4, the increasing addition of AAP_yP_hE gradually decreases the glass transition temperatures (T_g) and thermal decomposition temperatures (T_{d5} and T_{d10}) of the films for all tested series, which is a general rule for aliphatic-containing polyimide and may be good for improving the processing performances of the intended intractable PIs. The addition of AAP_yP_hE generally increases the DMA

TABLE 4 The Thermal and Mechanical Properties of the PI Films

PIs	Thermal properties				Mechanical properties ^a			
	T_g^b (°C)	T_{d5} (°C)	T_{d10} (°C)	Char yield (%)	Tan δ (DMA)	TS (MPa)	EB (%)	TM (GPa)
OPI-0	253	478	534	54.2	1.15	89.3	9.26	1.35
OPI-5	248	498	546	56.5	1.35	109.2	8.33	1.70
OPI-10	246	462	538	55.2	1.12	170.7	10.05	2.28
OPI-20	239	438	524	54.6	1.21	108.2	9.47	1.35
OPI-30	233	407	506	56.6	1.28	106.2	10.82	1.29
OPI-50	219	376	451	52.8	1.15	91.1	8.43	1.49
FPI-0	295	503	537	53.7	1.43	68.3	7.93	0.97
FPI-20	267	394	509	52.2	1.12	105.9	8.97	1.30
PPI-0	267	498	554	59	0.60	80.1	11.93	1.05
PPI-20	252	414	532	57.9	0.23	30.5	9.06	0.66
TPI-0	283	473	544	56.6	1.09	116.0	11.8	1.49
TPI-20	282	425	526	57.1	0.36	74.7	7.94	1.07

^a TS, tensile strength; EB, elongation at break; TM, tensile modulus.

^b Tested by DMA heated at 5 °C min⁻¹ in N₂.

tan δ value of ODA-ODPA films as compared by the cases of OPI- x ($x = 5-50$) to OPI-0. OPI-5 has the biggest tan δ value of 1.35 and this may be attributed to the introduction of flexible aliphatic ethylene segments. However, the tan δ values of PIs from OPI-10 to OPI-50 present a complex fluctuation. Initially, the intermolecular cross-linking structure by condensation of hydroxyl groups leads to a sharp decrease of tan δ of OPI-10. When the molar content of AAP_{*y*}P_{*h*}E further increases, the condensation of hydroxyls becomes difficult and the increasing presence of flexible aliphatic ethylene segments results in the increase of tan δ for OPI-20 and OPI-30. However, when the presence of free hydroxyl groups continues to increase with the increasing addition of AAP_{*y*}P_{*h*}E, the interchain hydrogen bond formation becomes available and that makes the polymer rigid again, as indicated by the decrease of the tan δ value of OPI-50.

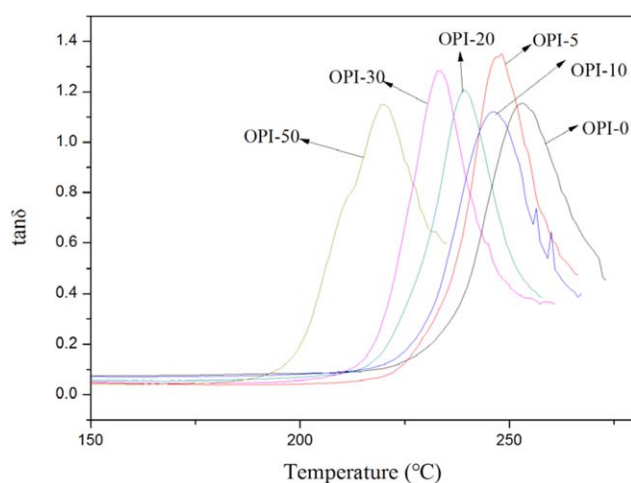


FIGURE 8 The DMA curves of the OPI- x films. [Color figure can be viewed at wileyonlinelibrary.com]

Cross-linking correlates with the viscoelastic properties of the polymers.³⁴ Lu and Larock calculated the cross-linking density based on the equation $E' = 3\nu_e RT$, where E' is the storage modulus at $T_g + 40$ °C, R is the gas constant, T is the absolute temperature at $T_g + 40$ °C, and ν_e is the cross-linking density.³⁵ Meanwhile, they introduced the soluble fraction (SF) in DMF to estimate the cross-linking degree of the soybean oil-based polymers containing different content of hydroxyls which react with functional cyanate groups to build cross-linking. According to their methods, we obtained the ν_e and SF values for the OPI- x samples from OPI-0 to OPI-50 based on the DMA storage modulus in Figure 9 and the SF detection method described in Measurements, and the results are summarized in Table 5.

Seen in Table 5, the change of SF values are inversely proportional to that of the cross-linking density ν_e for OPI- x series. It shows that OPI-0 has smaller ν_e than the rest of

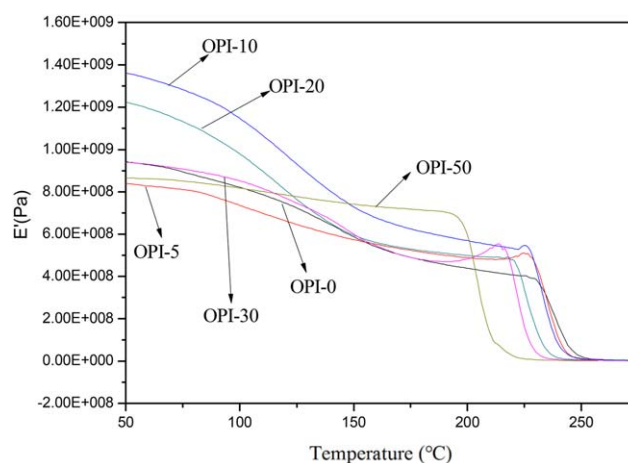


FIGURE 9 The storage modulus of the OPI- x films. [Color figure can be viewed at wileyonlinelibrary.com]

TABLE 5 The ν_e and SF Values of OPI-x Films

Code	E' (Pa)	ν_e (mol/m ³)	SF (%)
OPI-0	565578	40.1	31.69
OPI-5	1678727.3	119.9	26.02
OPI-10	2073718	148.7	16.52
OPI-20	1735257.6	126.1	18.65
OPI-30	1484370.9	109.1	34.25
OPI-50	718846.9	54.2	28.37

OPI-x films, indicating the introduction of AAP_yP_hE leads to cross-linking structure. It is also found that the cross-linking density changes in a fluctuated manner with the increasing loading of AAP_yP_hE for OPI-x films.

Dielectric Properties of the Copolymer Films

To elucidate the influence of AAP_yP_hE to the dielectric properties of PIs, the dielectric constant (ϵ') and dielectric loss (ϵ'') of OPI-x series with different content of AAP_yP_hE were studied as the function of frequency and temperature.

Dielectric Constant (ϵ')

Figure 10 shows the dielectric constant (ϵ') versus frequency and temperature three-dimensional diagram of OPI-20. It can be seen that ϵ' generally increases with increasing temperature and there exist some relaxations that are similar to the dielectric loss later presented in this article.³⁶ ϵ' variation with frequency is determined by the ability of the dipoles in polymer to move fast enough for their orientation to keep pace with the increased oscillations in an alternating electric field.³⁷⁻³⁹ With the frequency increasing, the orientational polarization of the dipoles would gradually lose pace with the alternation of the applied electric field, and so the ϵ' value of the PI films would decrease, and this tendency

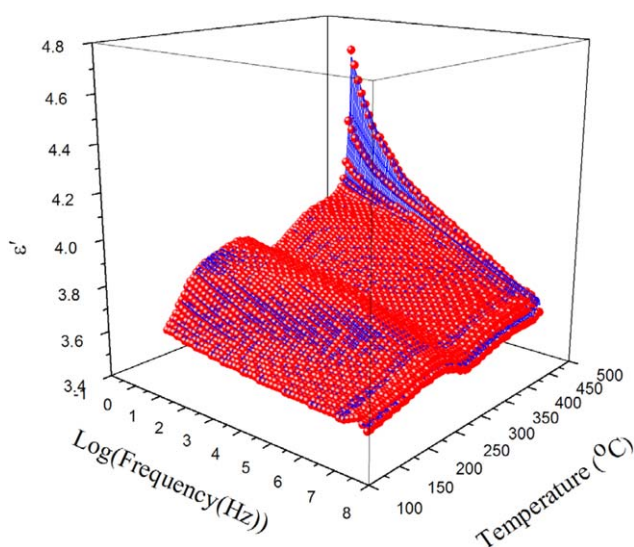


FIGURE 10 The dielectric constant (ϵ') versus frequency and temperature for OPI-20. [Color figure can be viewed at wileyonlinelibrary.com]

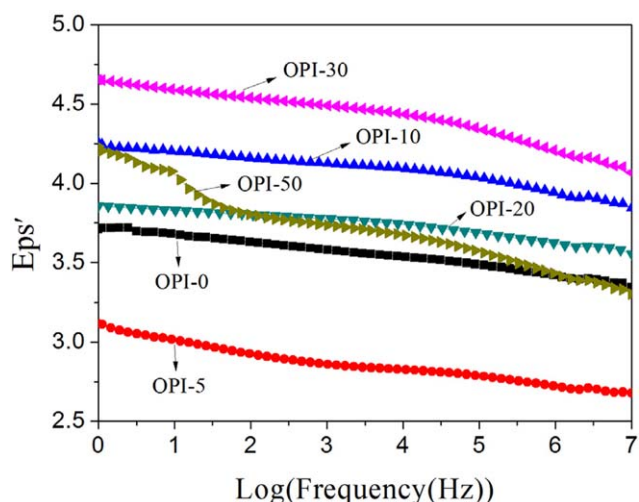


FIGURE 11 The dielectric constant (ϵ') versus frequency for OPI-x films. [Color figure can be viewed at wileyonlinelibrary.com]

becomes more obvious at higher frequency, as shown by Figure 11.

As shown in Table 6, OPI-5 has the lower ϵ' than OPI-0, as the incorporation of aliphatic structure reduces the electron polarization and inhibits the CTC. However, as the molar content of AAP_yP_hE increase, the ϵ' value of OPI-10 presented an increase, which may be due to the increasing presence of polar hydroxyl groups that has offset the dielectric constant-reducing effect of the alicyclic ethylene segments. With the molar content of AAP_yP_hE continues to increase to 20% (OPI-20), the ϵ' reverses to decrease. It is understood that during the thermal treatment of the film preparation process, the increasing number of hydroxyls would condense to create a cross-linked structure of the polymer. This reversal at OPI-20 could be the synergistic effect of the aliphatic ethylene structure and the cross-linking structure. When the molar content of AAP_yP_hE increase to 30%, the rigid cross-linking polymer chains would restrict the free motion of the hydroxyls and so make further condensation difficult, leading to some exposed hydroxyls. Hence, the increased presence of polar hydroxyls contributes to an increase in the ϵ' of OPI-

TABLE 6 Dielectric Constant of OPI-x Films with Varied Frequency at 25 °C

PIs	Dielectric constant (ϵ')			
	1 Hz	1 kHz	1 MHz	10 MHz
OPI-0	4.61	4.48	4.32	4.24
OPI-5	4.02	3.76	3.62	3.57
OPI-10	5.15	5.02	4.84	4.74
OPI-20	4.76	4.67	4.52	4.45
OPI-30	5.55	5.39	5.11	4.96
OPI-50	5.13	4.64	4.33	4.20

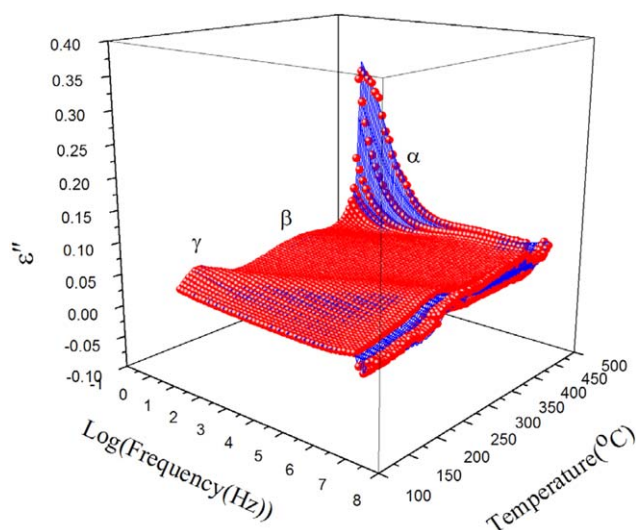


FIGURE 12 The dielectric loss (ϵ'') versus frequency and temperature for OPI-20. [Color figure can be viewed at wileyonlinelibrary.com]

30. Nevertheless, when the molar content of $\text{AAP}_y\text{P}_h\text{E}$ continues to increase, the increasing number of exposed hydroxyls may form hydrogen bond and lead to secondary weak crosslinking structure, leading to a decrease of the ϵ' for OPI-50.

Dielectric Loss (ϵ'')

The dielectric loss (ϵ'') is one of the important indexes to evaluate the quality of the insulating material. It is decided by the energy loss caused by the molecular dipoles orientational polarization and the intrinsic friction of electron transfer.³⁷ The frequency and temperature dependences of the ϵ'' for OPI-20 is shown in Figure 12. Basically similar to ϵ' change tendency, the ϵ'' increased with increasing temperature, and three relaxation processes designated as γ , β , and α , respectively, are observed for the ϵ'' variation with increasing temperature. We have reported these relaxations in our previous work.³⁰ Generally, the ϵ'' decreases with the increasing frequency over the frequency range tested, but, as shown in Supporting Information, Figure S10, there appeared some unreported relaxations on which we will conduct further investigation in future.

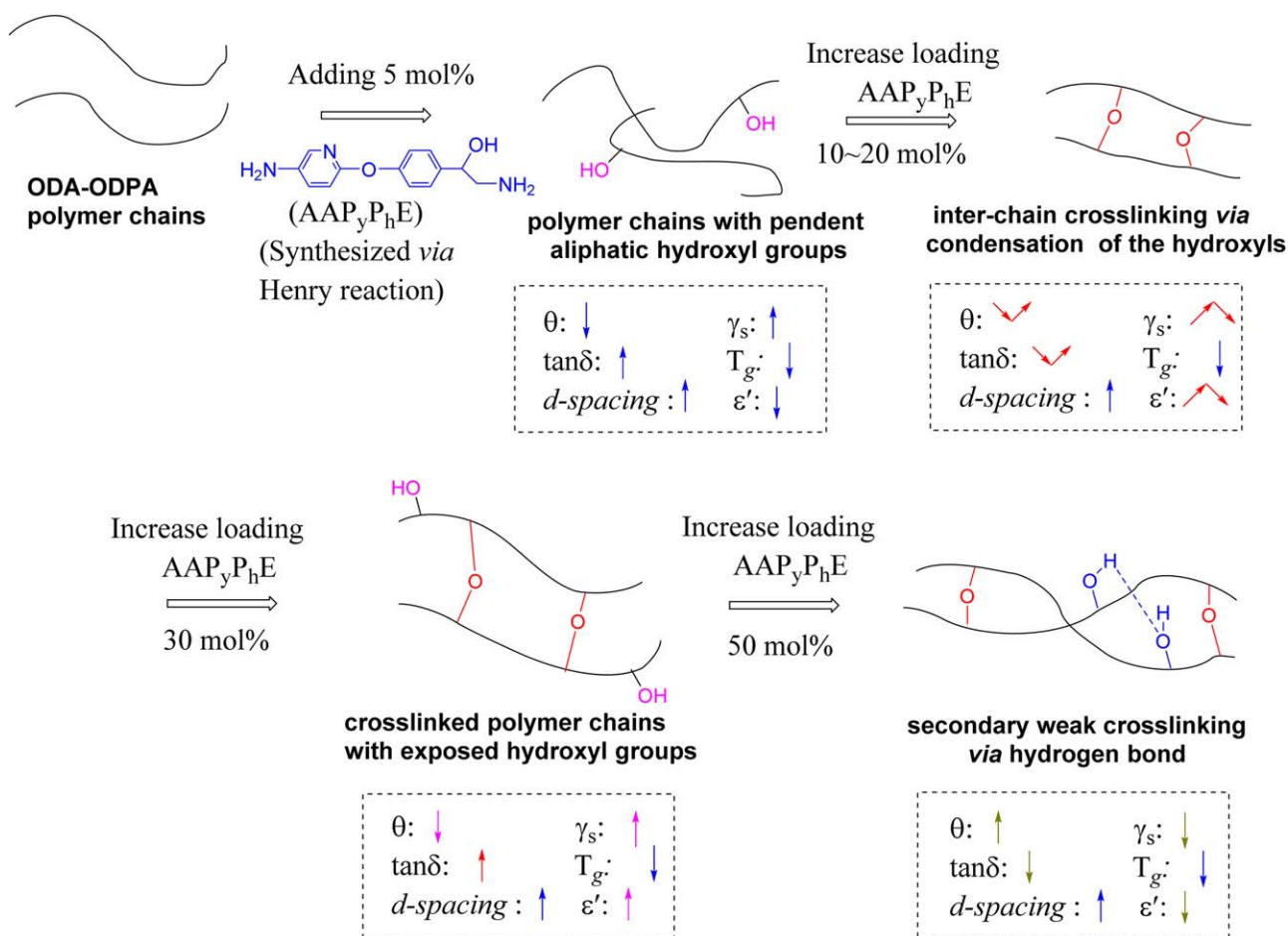


FIGURE 13 The proposed copolymer interchain structures with the variation of the loading of aliphatic hydroxyl-containing $\text{AAP}_y\text{P}_h\text{E}$. [Color figure can be viewed at wileyonlinelibrary.com]

CONCLUSIONS

In this work, a novel asymmetric hydroxyl-containing aliphatic–aromatic diamine AAP_yP_hE was facily synthesized by way of Henry reaction in three steps. Preliminary screening on different aromatic dianhydrides reveals the desirable condensation reactivity of ODPa toward AAP_yP_hE. Furthermore, comparative investigations show that the incorporation of AAP_yP_hE improves the solubility and optical transparency by inhibiting CTC and reducing the chain packing due to the asymmetric structure and aliphatic ethylene segments, and meanwhile retains the inherent thermal and mechanical properties of the polymers. The molar content of the incorporated AAP_yP_hE was found to have fluctuated influences on the film surface water contact properties such as θ and γ_s , and the similar effects of the variation of molar content of AAP_yP_hE were observed on the DMA $\tan \delta$ and dielectric constant ϵ' .

We proposed that with the increase of molar content of AAP_yP_hE, the increasing hydroxyl groups would lead the polymer chain structure to four different stages as outlined in Figure 13. It is postulated that when the molar content of AAP_yP_hE reaches certain value, the pendent alicyclic hydroxyl would condense to form interchain cross-linked network. On increasing addition of AAP_yP_hE, the cross-linked polymer would bear some exposed hydroxyl groups because the rigid polymer chain restricted the free motion of the pendent hydroxyls. Further increase of AAP_yP_hE leads to increasing presence of pendent hydroxyls that would tend to form secondary interchain weak cross-linking by hydrogen bond.

ACKNOWLEDGMENTS

The financial supports from the NSFC (Grant Nos. 51263014 and 21271099) and Jiangxi Provincial Education Department (Grant No. GJJ13113) are greatly appreciated. The authors are thankful to Prof Haoqing Hou from Jiangxi Normal University, China for kindly providing DMA measurements of all these samples.

REFERENCES AND NOTES

- (a) M. K. Ghosh, K. L. Mittal, *Polyimides: Fundamentals and Applications*; Marcel Decker: New York, **1996**, p1; (b) C. E. Stroog, *History of the Invention and Development of the Polyimides*; Plastics Engineering: New York, **1996**.
- (a) G. Maier, *Prog. Polym. Sci.* **2001**, *26*, 3; (b) H. Lim, W. J. Cho, C. S. Ha, S. Ando, Y. K. Kim, C. H. Park, K. Lee, *Adv. Mater.* **2002**, *14*, 1275.
- Y. W. Liu, C. Qian, L. J. Qu, Y. N. Wu, Y. Zhang, X. H. Wu, B. Zou, W. X. Chen, Z. Q. Chen, Z. G. Chi, S. W. Liu, X. D. Chen, J. R. Xu, *Chem. Mater.* **2015**, *27*, 6543.
- Z. X. Zhou, Y. Zhang, S. W. Liu, Z. G. Chi, X. D. Chen, J. R. Xu, *J. Mater. Chem. C* **2016**, *4*, 10509.
- A. S. Mathews, I. Kim, C. S. Ha, *Macromol. Res.* **2007**, *15*, 114.
- H. J. Ni, J. G. Liu, Z. H. Wang, S. Y. Yang, *J. Ind. Eng. Chem.* **2015**, *28*, 16.
- X. J. Zhao, J. G. Liu, H. S. Li, L. Fan, S. Y. Yang, *J. Appl. Polym. Sci.* **2009**, *111*, 2210.

- H. C. Yu, S. V. Kumar, J. H. Lee, S. Y. Oh, C. M. Chung, *Macromol. Res.* **2015**, *23*, 566.
- D. J. Liaw, C. C. Huang, W. H. Chen, *Macromol. Chem. Phys.* **2006**, *207*, 434.
- A. S. Mathews, L. L. Kim, C. S. Ha, *J. Polym. Sci. Part A: Polym. Chem.* **2006**, *44*, 5254.
- K. Goto, T. Akiike, Y. Inoue, M. Matsubara, *Macromol. Symp.* **2003**, *199*, 321.
- X. D. Ji, Z. K. Wang, J. L. Yan, Z. Wang, *Polymer* **2015**, *74*, 38.
- Y. Guan, D. M. Wang, G. L. Song, G. D. Dang, C. H. Chen, H. W. Zhou, X. G. Zhao, *Polymer* **2014**, *55*, 3634.
- Y. Shao, Y. F. Li, X. Zhao, X. L. Wang, T. Ma, F. C. Yang, *J. Polym. Sci. Part A: Polym. Chem.* **2006**, *44*, 6836.
- C. Y. Wang, W. T. Chen, C. Xu, X. Y. Zhao, J. Li, *Chin. J. Polym. Sci.* **2016**, *34*, 1363.
- P. K. Tapaswi, M. C. Choi, Y. S. Jung, H. J. Cho, D. J. Seo, C. S. Ha, *J. Polym. Sci. Part A: Polym. Chem.* **2014**, *52*, 2316.
- W. Volksen, H. J. Cha, M. I. Sanchez, D. Y. Yoon, *React. Funct. Polym.* **1996**, *30*, 61.
- J. A. Kreuz, B. S. Hsiao, C. A. Renner, D. L. Goff, *Macromolecules* **1995**, *28*, 6926.
- T. Namikoshi, K. Odahara, A. Wakino, M. Murat, S. Watanabe, *High Perform. Polym.* **2015**, *27*, 183.
- K. Itoya, Y. Kumagai, M. Kakimoto, Y. Imai, *Macromolecules* **1994**, *27*, 4101.
- T. Ogura, M. Ueda, *Macromolecules* **2007**, *40*, 3527.
- C. Koninga, A. Delmottea, P. Larnoa, B. V. Mele, *Polymer* **1998**, *39*, 3697.
- A. E. Eichstadt, T. C. Ward, M. D. Bagwell, I. V. Farr, D. Dunson, J. E. McGrath, *J. Polym. Sci. Part B: Polym. Phys.* **2002**, *40*, 1503.
- Y. Watanabe, Y. Sakai, Y. Shibasaki, S. Ando, M. Ueda, *Macromolecules* **2002**, *35*, 2277.
- Y. Guan, C. B. Wang, D. M. Wang, G. D. Dang, C. H. Chen, H. W. Zhou, X. G. Zhao, *Polymer* **2015**, *62*, 1.
- C. B. Wang, X. G. Zhao, D. B. Tian, D. M. Wang, C. H. Chen, H. W. Zhou, *Des. Monomers Polym.* **2017**, *20*, 97.
- B. Jarzabek, E. Schab-Balcerzak, T. Chamenko, D. Sęka, J. Cisowska, A. Volozhin, *J. Non-Cryst. Solids* **2002**, *2*, 1057.
- Y. T. Chern, H. C. Shiue, *Macromolecules* **1997**, *30*, 4646.
- Noboru Ono, *The Nitro Group in Organic Synthesis*; Wiley-VCH, **2001**; Chapter 3, p 30.
- J. O. Osby, B. Ganem, *Tetrahedron Lett.* **1985**, *26*, 6413.
- Q. Q. Bu, S. J. Zhang, H. Li, Y. F. Li, C. L. Gong, F. C. Yang, *Polym. Degrad. Stab.* **2011**, *96*, 1911.
- J. Li, H. S. Zhang, F. Liu, J. C. Lai, H. X. Qi, X. Z. You, *Polymer* **2013**, *54*, 5673.
- J. S. Tian, H. Y. Wang, Z. Y. Huang, R. G. Lu, P. H. Cong, X. J. Liu, T. S. Li, *J. Macromol. Sci. B Phys.* **2010**, *49*, 791.
- R. Hagen, L. Salmen, B. Stengerg, *J. Polym. Sci. Part B: Polym. Phys.* **1996**, *34*, 1997.
- Y. S. Lu, R. C. Larock, *Biomacromolecules* **2008**, *9*, 3332.
- S. Ebisawa, J. Ishiia, M. Sato, L. Vladimirov, M. Hasegawa, *Eur. Polym. J.* **2010**, *46*, 283.
- F. Li, J. C. Lai, W. J. Wan, F. Liu, H. X. Qi, X. S. Li, X. Z. You, *J. Appl. Polym. Sci.* **2015**, *132*, 42670.
- M. Ree, K. Kim, S. H. Woo, H. Chang, *J. Appl. Polym. Sci.* **1997**, *81*, 698.
- G. C. Eastmond, J. Paprotny, R. A. Pethrick, S. M. Fernan, *J. Appl. Polym. Sci.* **2015**, *132*, 41684/1.